Tellus SERIES B CHEMICAL AND PHYSICAL METEOROLOGY
PUBLISHED BY THE INTERNATIONAL METEOROLOGICAL INSTITUTE IN STOCKHOLM

Tellus (2009), 61B, 566–576
Printed in Singapore. All rights reserved

TELLUS

Atmospheric circulation controls on precipitation isotope–climate relations in western Canada

By S. J. BIRKS[1,2]* and T. W. D. EDWARDS[2], [1]*Alberta Research Council, 3608-33 Street NW, Calgary, AB T2L 2A6, Canada;* [2]*Earth and Environmental Sciences, University of Waterloo, Waterloo, ON N2L 3G1, Canada*

(Manuscript received 25 August 2008; in final form 31 March 2009)

ABSTRACT

$\delta^{18}O$ and $\delta^{2}H$ time-series of monthly composite precipitation (July 1975–June 1982) for three stations located in western Canada were examined to characterize the influence of atmospheric circulation on modern isotope–climate relations in the region. Spatially coherent trends in long-term isotope and temperature anomalies were evident among the three stations, with isotope and temperature anomalies showing the strongest correlations when weighted to reflect precipitation amount. Strong correlations were also found between unweighted isotope anomalies and the Pacific–North American (PNA) index, which is a key descriptor of air-mass circulation patterns across North America. Positive δ anomalies and variable temporal δ–temperature relations having relatively shallow slopes occur during periods of intensified meridional circulation (PNA+), especially during winter. Periods of stronger zonal circulation (PNA−), in contrast, are marked by negative δ anomalies and steeper δ–temperature relations, consistent with increased distillation and deepening of the isotope shadow in the lee of the Canadian Cordillera. Significant positive correlations with pressure-height and precipitable-water anomalies located over western Canada provide additional confirmation that seasonal and interannual variability in the strength of the PNA ridge-and-trough pattern profoundly influences the isotopic evolution of moisture reaching the interior. Analogous circulation-dependent shifts in the precipitation isotope–temperature relation in western Canada also occur over much longer timescales, as inferred from isotope palaeorecords in various natural archives.

1. Introduction

The stable-isotope composition of precipitation integrates a variety of factors, including temperature and precipitation amount at the site of deposition, as well as conditions upstream, where vapour originates and during its subsequent atmospheric transport and distillation (Dansgaard, 1964; Rozanski et al., 1993). Identifying and disentangling the relative importance of these factors on temporal and spatial variability in the isotopic composition of precipitation is necessary to properly interpret climate signals preserved in natural isotopic archives like ground water, glacier ice, lake sediments and tree rings. Characterizing relations between the $\delta^{18}O$ (or $\delta^{2}H$)[1] of precipitation and temperature is of particular importance because of its potential application as an 'isotopic palaeothermometer' (Jouzel, 1999).

Limitations on the traditional interpretation of precipitation $\delta^{18}O$ as an isotope thermometer at mid- and high latitudes have been identified conceptually (Fricke and O'Neil, 1999) and in studies of the rainout history, seasonality and changing vapour source areas for modern precipitation (e.g. Lawrence and White, 1991; Simpkins, 1995; Kohn and Welker, 2005; Moran et al., 2007; Holdsworth, 2008a,b). Various palaeoprecipitation archives also preserve evidence of apparent circulation-dependent variability in the isotopic composition of precipitation (Plummer, 1993; Amundson et al., 1996; Lipp et al., 1996; Edwards et al., 1996, 2008; Salamatin et al., 1998; Jouzel, 1999; Smith and Hollander, 1999; Teranes and McKenzie, 2001; Hammarlund et al., 2002; Hammarlund and Edwards, 2008), as do simulations by general and regional circulation models equipped with water-isotope tracer diagnostics (Cole et al., 1993; Noone and Simmonds, 1998, 2002; Werner et al., 2000; Hoffmann et al., 2001; Werner and Heimann, 2002; Sturm et al., 2005, 2007; Lee et al., 2007).

Here we report a detailed analysis of isotope–climate relations in time-series of monthly composite $\delta^{2}H$, $\delta^{18}O$ and *d*-excess ($=\delta^{2}H - 8\delta^{18}O$) obtained from three stations in the northern Great Plains of western Canada between 1 July 1975 and 30 June 1982. Our results demonstrate that systematic variability in

*Corresponding author.
e-mail: Jean.birks@arc.ab.ca
DOI: 10.1111/j.1600-0889.2009.00423.x
[1]The stable-isotope composition of precipitation is conventionally expressed as $\delta^{18}O$ or $\delta^{2}H$ values, such that $\delta_{precipitation} = ((R_{precipitation}/R_{VSMOW}) - 1) \times 1000$ ‰, where R represents the respective $^{18}O/^{16}O$ or $^{2}H/^{1}H$ ratios in precipitation and Vienna Standard Mean Ocean Water.

the isotopic composition of precipitation in the region occurred in response to changes in the pattern of large-scale atmospheric circulation during this interval, including characteristic fluctuations in temporal δ–temperature relations that are consistent with inferences from palaeo-isotope records. These results support the notion that water-isotope signals inherited from palaeo-precipitation may contain important information about changes in past synoptic climatology, in addition to temperature.

2. Climatological setting

The three stations used in this study—Gimli (50°38′N; 97°00′W), The Pas (53°49′N; 101°15′W) and Wynyard (51°46′N; 104°11′W)—are all located in the prairie climate region of southcentral Canada, spanning ∼3° latitude (∼350 km) and ∼7° longitude (∼500 km). More specifically: Gimli (221 m asl), the most southerly and easterly station, lies in the interlake area of southern Manitoba within the subhumid low Boreal ecoclimatic region; The Pas (271 m asl), the northernmost station, lies within westcentral Manitoba in the subhumid Mid Boreal (MBs) region; and Wynyard (561 m asl) lies in southeastern Saskatchewan within the Transitional Grasslands region (Ecoregions Working Group, 1989). As revealed by Fig. 1, the three stations experience very similar local meteorological regimes marked by strong seasonality in temperature and precipitation, with ∼60% or more of the latter falling as rain during the thaw season.

Mid-tropospheric circulation across Canada is characterized by the persistence of a large-scale ridge-and-trough pattern. The Pacific–North American (PNA) index, calculated using centres of action over the North Pacific and North America (Wallace and Gutzler, 1981) or alternatively from the empirical orthogonal function (EOF) of geopotential height anomalies, can be used to describe the strength or weakness of this pattern across the continent. Positive PNA index values are associated with a strengthening of the western North American ridge and eastern North American trough, resulting in more meridional flow, whereas negative PNA index corresponds with weakening of the ridge-and-trough pattern and intensified zonal flow. The PNA pattern is the first principal component of Northern Hemisphere circulation in January (Davis and Benkovic, 1994) and a major component throughout autumn, winter and spring (Barnston and Livezey, 1987).

3. Methods

The Global Network for Isotopes in Precipitation database (IAEA/WMO, 2006) contains the δ^{18}O and δ^{2}H values for composite monthly precipitation samples collected in an experimental monitoring campaign between July 1975 and June 1982 (84 months) from Gimli, The Pas and Wynyard (see Fritz et al., 1987). Climate parameters for the three stations were obtained from meteorological stations operating at each of the sites (mean monthly and daily temperatures and precipitation amounts) as well as from the NCEP/NCAR reanalysis data set (Kalnay et al., 1996). Changes in air-mass circulation were evaluated using the PNA index derived from the second principal component of the EOF of Northern Hemisphere (20°–90°N) sea-level pressure-height covariance (1948–2003) based on the NCEP/NCAR reanalysis data set.

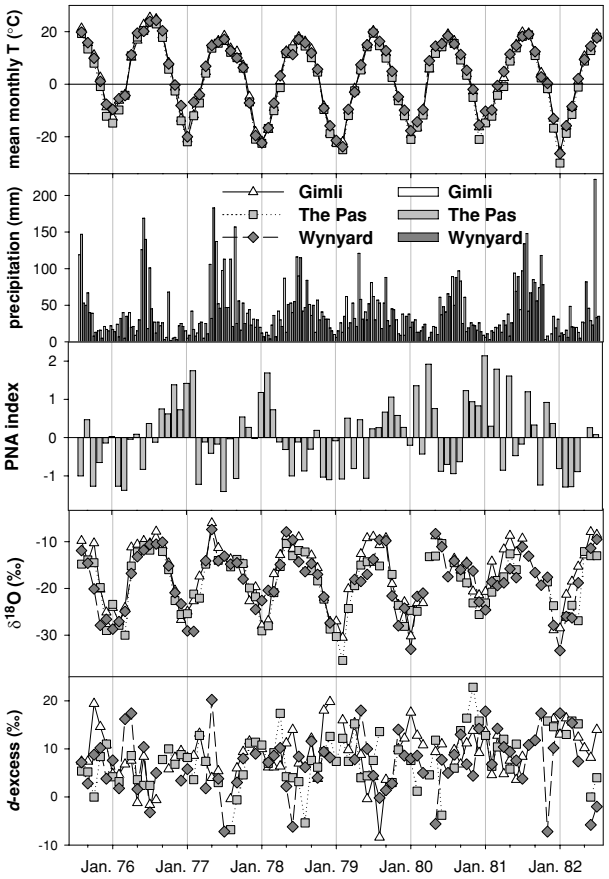

Fig. 1. Time-series of mean monthly temperature, total precipitation, PNA index and δ^{18}O and *d*-excess of precipitation for the study period.

Long-term monthly, seasonal and annual averages were calculated for precipitation δ^{18}O, δ^{2}H, *d*-excess and temperature time-series. Similar amount-weighted averages (w) were calculated for these parameters at each station according to

$$\bar{\delta}_W = \frac{\sum_{i=1}^{n} P_i \delta_i}{\sum_{i=1}^{n} P_i},$$

where P_i and δ_i are daily or monthly precipitation amount (mm) and the δ^{18}O, δ^{2}H or *d*-excess value (‰), respectively.

Forty-nine δ values are missing from 504 potential observations, due to lack of precipitation or sample loss, though only 12 out of 252 monthly observations lack both δ^{18}O and δ^{2}H. Missing δ values (23 δ^{18}O and 26 δ^{2}H) were filled using the long-term

average values at the respective site for the same months. The seasonal component of the monthly data was then removed by applying 12-month moving averages with and without precipitation amount weighting. Differences between each 12-month period and the long-term averages were calculated, yielding a time-series of the deviations (anomalies) of each parameter (Δ). It should be noted that the dates associated with each point on the Δ time-series correspond to the preceding 12-month period. Weighted temperature anomalies were calculated using both daily and monthly data, giving similar results. The daily data were used to calculate a monthly weighted average temperature so that the calculated monthly value only accounted for days in which precipitation occurred. These amount-weighted monthly values were then used in an amount-weighted, 12-month moving mean to derive the temperature anomaly time-series.

Temporal variations in the δ^{18}O–T relation were examined in more detail by performing 12-month moving linear regressions between the two parameters to determine how the slope, intercept and correlation coefficient of the relation varied over the study period.

Temporal correlation coefficients were calculated between an isotope-anomaly time-series for each station and gridded climate anomaly fields obtained from the NCEP/NCAR reanalysis data set. Gridded climate anomaly fields were calculated by subtracting climatological gridded monthly averages (1958–1997) from monthly data for the period. The station anomaly time-series was correlated to the time-series at each point in the gridded climate field, resulting in a two-dimensional grid of correlation values (the 95% significance level was evaluated using Student's t test, in which the population variances were assumed to be unequal).

4. Results

4.1. Time-series of climate and isotope data

The temperature, precipitation and isotope time-series for the three stations display the expected seasonal patterns (Fig. 1). For δ^{18}O (and δ^{2}H, not shown), this consists of a regular cycle between very negative values in winter and less negative values in summer. The isotopic compositions of precipitation at the three stations are remarkably similar even though the precipitation amounts differ. The d-excess time-series are far noisier (and less complete, given dependence on availability of both δ^{18}O and δ^{2}H) but also exhibit general seasonal patterns marked by higher values during the winter months and lower values in the summer. Linear regression of unweighted monthly δ^{18}O and δ^{2}H values for each station yields:

$$\text{Gimli}: \quad \delta^{2}\text{H} = 7.78\delta^{18}\text{O} + 6.22 \quad (r^2 = 0.983);$$

$$\text{ThePas}: \quad \delta^{2}\text{H} = 7.62\delta^{18}\text{O} + 0.62 \quad (r^2 = 0.989);$$

$$\text{Wynyard}: \quad \delta^{2}\text{H} = 7.63\delta^{18}\text{O} + 0.07 \quad (r^2 = 0.985).$$

The lower slopes and intercepts of the relations for Wynyard, and The Pas are perhaps attributable to greater influence from summer raindrop re-evaporation than at Gimli, situated in the slightly moister Interlake area, while all three equations yield essentially identical characterization of more depleted winter precipitation. In spite of the overall regularity in the annual cycles portrayed in Fig. 1, distinct interannual differences in climate and isotope parameters are evident. These can be explored in more detail by considering correlations between selected isotope and climate anomaly (Δ) time-series, as presented in Figs. 2–5 and Tables 1–4.

4.2. Correlations between isotope and climate anomalies

Significant correlations exist between the unweighted $\Delta\delta^{18}$O time-series at the three stations, as apparent visually from Fig. 2 (see also Table 1), verifying the existence of a spatially coherent regional isotope signal. Data from all three sites have positive δ^{18}O anomalies early in the time-series, followed by a switch to negative anomalies, reaching a minimum centred on the end of January 1979 and, finally, a return to positive $\Delta\delta^{18}$O values in the early 1980s. Warmer-than-average temperatures also occurred at all three stations at the beginning of the study period, followed by a general cooling until late 1979 and then a return to average temperatures (Fig. 2). However, the expected association of positive $\Delta\delta^{18}$O with positive ΔT is not consistently observed, as reflected also in the relatively low correlation coefficients ($r = 0.19$–0.49; Table 2). The precipitable water anomalies (ΔPWAT) are more variable and less strongly correlated among the three stations (Fig. 3); however, negative PWAT anomalies at all stations coincide with the isotope and temperature anomaly minima in 1979. The unweighted $\Delta\delta^{18}$O and ΔPWAT time-series consistently exhibit higher correlations ($r = 0.48$–0.54, Table 2) than between $\Delta\delta^{18}$O and ΔT, and visual comparison of the time-series indicates that ΔPWAT seems to better predict some of the small-scale features in the $\Delta\delta^{18}$O time-series, particularly during the later portions of the records. Significantly stronger and more consistent correlations exist between the individual time-series of unweighted δ^{18}O anomalies and the PNA index (Fig. 4), with positive isotope anomalies occurring at all stations during positive phases of the PNA and negative anomalies occurring during periods of negative PNA index ($r = 0.67$–0.79; Table 2). Remarkably, even many of the fine-scale features within the PNA record seem to be present in the isotope anomaly time-series. As revealed in Fig. 5, precipitation amount weighting notably strengthens the correlations between the δ^{18}O and T anomalies, while significantly weakening the correlations with the PNA index and variably influencing other isotope–climate anomaly correlations (Table 2). Overall, these various statistical relations clearly suggest that circulation-dependent factors play an important role in the isotopic labelling of precipitation in the study area.

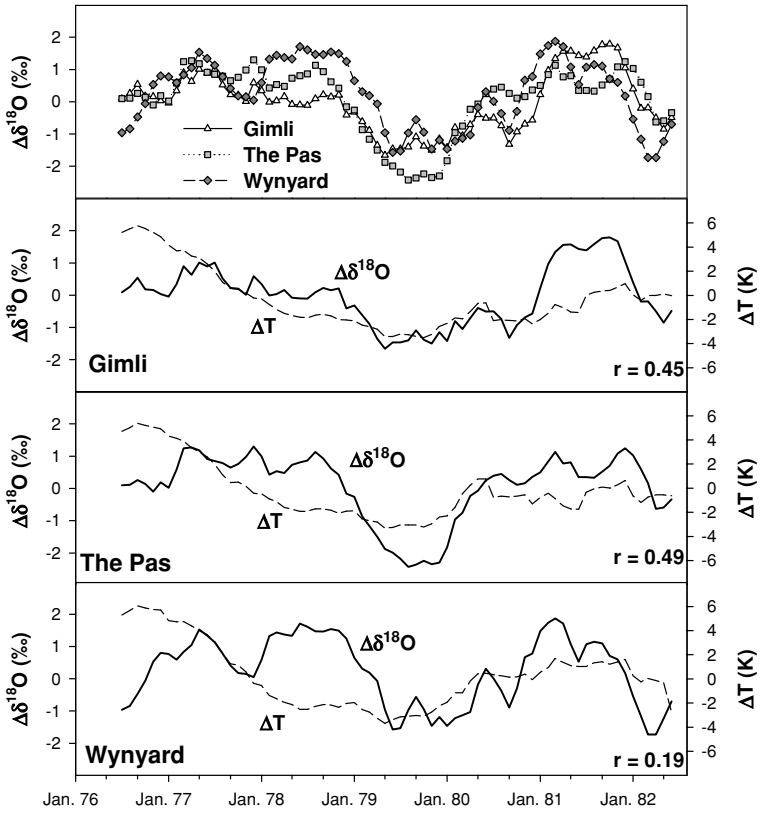

Fig. 2. Unweighted δ^{18}O anomaly ($\Delta\delta^{18}$O) time-series for each of the stations (top panel) and comparison between $\Delta\delta^{18}$O and unweighted temperature anomaly (ΔT) time-series for each site (lower panels).

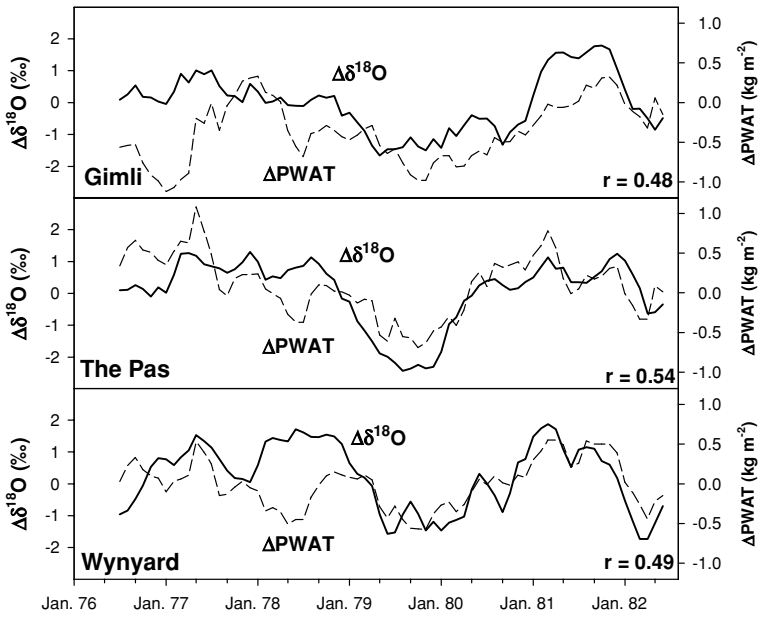

Fig. 3. Comparison of the unweighted $\Delta\delta^{18}$O time-series (see Fig. 2) with the precipitable water anomaly (ΔPWAT) time-series for each station.

Although not shown here, comparable correlations in all respects were obtained using the equivalent δ^2H anomaly time-series, and we hence restrict subsequent discussion to δ^{18}O, with selective consideration of *d*-excess. To see whether the relationships described above are applicable to other areas of the Great Plains over different time periods, similar correlations were determined using a 10-year record of monthly δ^{18}O precipitation data from Calgary, Alberta, collected between January 1992 and December 2001 (Peng et al., 2004). This slightly longer data set also had more significant correlations between isotope anomalies and the PNA index (unweighted $\Delta\delta^{18}$O vs. PNA, $r = 0.63$; weighted $\Delta\delta^{18}$O vs. PNA, $r = 0.55$) than with temperature.

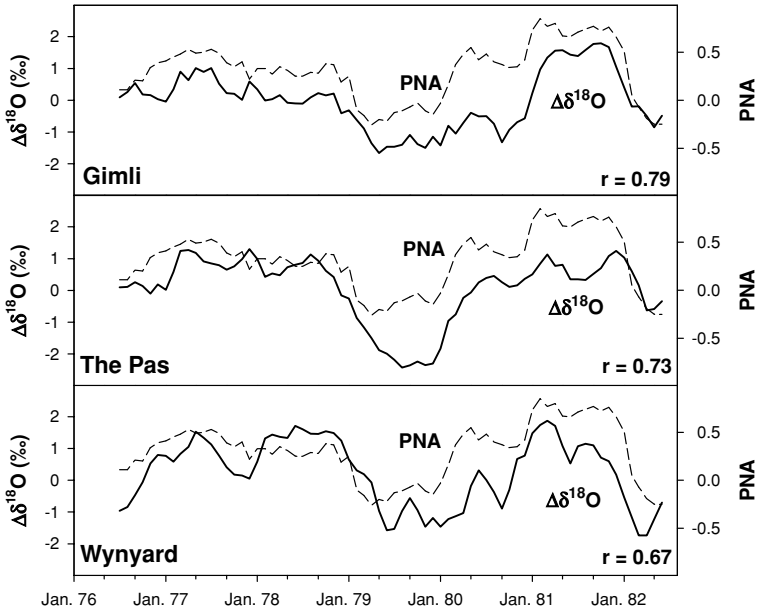

Fig. 4. Comparison of the unweighted $\Delta\delta^{18}O$ time-series (see Fig. 2) with the Pacific–North American pattern (PNA) index time-series for each station.

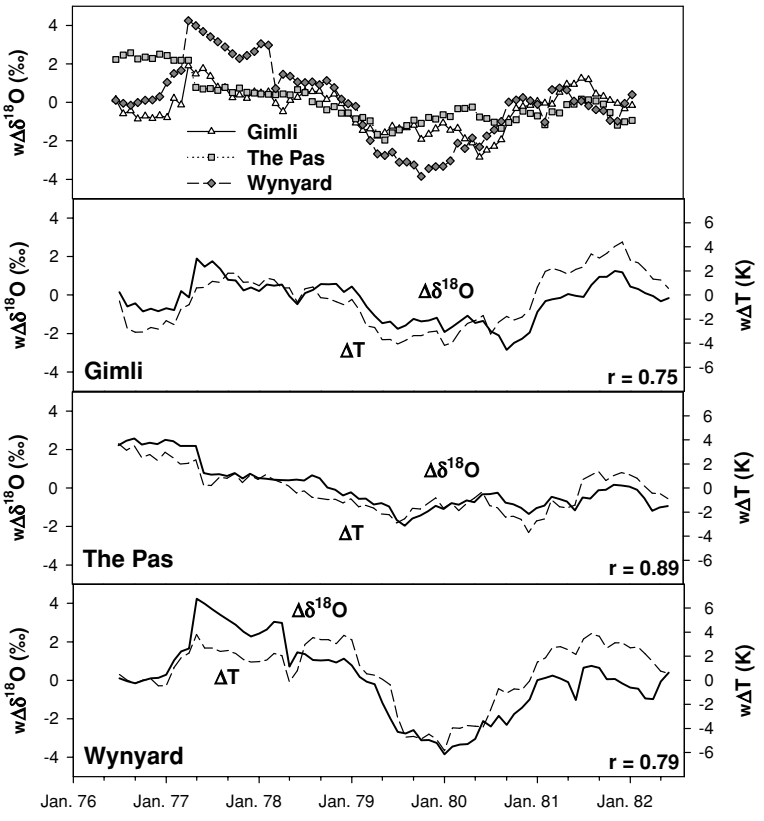

Fig. 5. Precipitation-amount-weighted isotope anomaly ($w\Delta\delta^{18}O$) time-series for each of the stations (top panel) and comparison between $w\Delta\delta^{18}O$ and weighted temperature anomaly ($w\Delta T$) time-series for each site (lower panels).

4.3. Correlations between isotope anomalies and gridded climate fields

Correlations between station isotope anomaly time-series and gridded climate data (Fig. 6) also help to characterize isotope–climate relations in this region. For example, areas of significant positive correlation between the $\delta^{18}O$ anomaly time-series for each of the stations and the gridded 500 mbar geopotential height anomaly (Δ500 mbh) field are very similar to the geopotential height anomalies that define the PNA index, thus, further

Table 1. Correlations between the δ^{18}O and *d*-excess anomaly time-series for each station

	Gimli vs. the Pas (*I*)	Gimli vs. Wynyard (*r*)	The Pas vs. Wynyard (*r*)
$\Delta\delta^{18}$O	0.77	0.65	0.67
Δd-excess	0.41	0.29	0.82

Note: Using a simple *t*-test (and 70 degrees of freedom) our correlation values become significant at the 95% level when the absolute value of *r* is greater than 0.23.

Table 2. Correlations between time-series of precipitation isotope anomalies and climate parameters for each station

	Gimli (*r*)	The Pas (*r*)	Wynyard (*r*)
Unweighted			
$\Delta\delta^{18}$O vs. ΔT	0.49	0.45	*0.19*
$\Delta\delta^{18}$O vs. ΔPWAT	0.54	0.48	0.49
$\Delta\delta^{18}$O vs. PNA	0.79	0.73	0.67
$\Delta\delta^{18}$O vs. % rain	0.57	0.64	0.50
Δd-excess vs. ΔT	−0.70	−0.31	*0.02*
Δd-excess vs. ΔPWAT	0.25	*−0.09*	0.29
Δd-excess vs. PNA	−0.27	*0.21*	*0.12*
Weighted			
w$\Delta\delta^{18}$O vs. wΔT	0.75	0.89	0.79
w$\Delta\delta^{18}$O vs. ΔPWAT	0.60	0.60	0.32
w$\Delta\delta^{18}$O vs. PNA	0.34	*0.23*	0.32
w$\Delta\delta^{18}$O vs. % rain	0.49	0.42	0.72
wΔd-excess vs. wΔT	−0.40	−0.45	*0.25*
wΔd-excess vs. ΔPWAT	*−0.20*	−0.37	0.33
wΔd-excess vs. PNA	*−0.22*	0.24	*0.22*
Selected			
PNA vs. ΔT	0.26	0.32	0.48
PNA vs. wΔT	0.55	*0.20*	0.44
PNA vs. ΔPWAT	0.34	0.62	*0.05*
PNA vs. % rain	0.30	0.40	0.32
ΔT vs. ΔPWAT	*−0.07*	0.72	0.56
ΔT vs. % rain	*−0.06*	0.44	*0.16*
wΔT vs. ΔPWAT	0.60	0.46	0.56
wΔT vs. % rain	0.93	0.59	0.95

Note: Correlations not significant at the 95% level are italicized.

supporting the idea that the strength of the PNA ridge-and-trough pattern affects local precipitation isotope signals. Correlation between the station $\Delta\delta^{18}$O time-series and ΔPWAT field reveals analogous results, although differences in the distribution and strength of the correlation fields emphasizes that other factors must affect the isotopic labelling process, despite the relative proximity of the three stations and the presence of a strong regional isotope signal in precipitation.

4.4. Synoptic examples

We can also probe the conditions that result in isotope anomalies and the correlation with the strength of the PNA pattern by considering the associated synoptic conditions during specific periods. As shown in Fig. 7, for example, the ridge-and-trough pattern was far more pronounced in January 1981 (PNA = +2.14) than in February 1979 (PNA = −1.08). The $\Delta\delta^{18}$O distributions for these two months were also markedly different, with positive isotope anomalies in the study area corresponding to meridional circulation in January 1981 and negative isotope anomalies corresponding to intensified zonal circulation during February 1979. Atmospheric moisture from the Pacific was transported predominantly eastwards across the southern Canadian Cordillera into the interior plains during February 1979. Meridional flow in January 1981, on the other hand, led to transport of moisture northward along the coast, before penetrating eastward across the Cordillera at lower elevation, thus, evidently undergoing less isotopic distillation prior to deposition in the study area than occurred when flow was more zonal.

Characteristic fluctuations in the temporal isotope–temperature relations at each of the stations can also be discerned in response to varying circulation regime. As shown in Tables 3 and 4, linear regression of the long-term δ^{18}O–*T* relations at each of the sites yields average slope coefficients of 0.39–0.43 ‰ K^{-1}, yet regression of 12-month moving averages reveals systematic variability between maxima of 0.52–0.57 ‰ K^{-1} and minima of 0.20–0.26 ‰ K^{-1} during this period, correlated inversely to the PNA index. This effect is particularly well marked for Gimli and The Pas (respective *r* values of −0.56 and −0.67) and can be clearly illustrated by comparing two 12-month intervals at Gimli, characterized by differing average PNA indices (Fig. 8). The 12-month interval ending April 1981, having predominantly meridional flow (average PNA = +0.49), has a shallow and statistically relatively weak δ^{18}O–*T* relation (slope = 0.28 ‰K^{-1}; $r = 0.70$), whereas the 12-month interval ending June 1979, having more zonal flow (average PNA = −0.48), has a steeper and statistically stronger δ^{18}O–*T* relation (slope = 0.48 ‰K^{-1}; $r = 0.98$). Notably, the temperature-dependent difference in isotopic labelling is primarily restricted to winter precipitation, as shown by convergence of the two relations at about 10 °C.

5. Discussion

5.1. Modern isotope climatology

The positive correlation between the time-series of PNA and unweighted $\Delta\delta^{18}$O (Fig. 4) suggests that when the ridge over the

Table 3. Statistics from the 12-month moving regressions of the δ^{18}O–T relations

	Slope δ^{18}O–T Relation		Intercept δ^{18}O–T Relation		r^2 δ^{18}O–T Relation	
	Long-term	12-month	Long-term	12-month	Long-term	12-month
Gimli	0.43	min. = 0.26	−17.66	−15.28	0.80	0.40
		max. = 0.54		−20.40		0.96
The Pas	0.40	min. = 0.26	−19.01	−17.39	0.83	0.63
		max. = 0.52		−21.69		0.96
Wynyard	0.39	min. = 0.20	−19.51	−16.86	0.72	0.50
		max. = 0.57		−23.95		0.96

Table 4. Correlations between regression statistics (Table 3) and the PNA index

	Gimli (r)	The Pas (r)	Wynyard (r)
Residuals (r^2) vs. PNA	−0.64	−0.27	−0.39
Slope vs. PNA	−0.56	−0.67	−0.21
Intercept vs. PNA	0.54	0.62	0.22

Rockies is more pronounced (i.e. mid-tropospheric flow is more meridional across western Canada), the northern Great Plains region receives isotopically enriched precipitation compared with times when flow is more zonal. This relation appears to be strongest in winter, when the δ^{18}O–T relation has the greatest variability. The significantly weaker relation between the PNA and weighted isotope anomaly (w$\Delta\delta^{18}$O) time-series (Table 2) is also consistent with this winter bias, reflecting suppression of the signal by abundant thaw-season precipitation, which is not strongly influenced isotopically by the PNA (Fig. 8). Additional

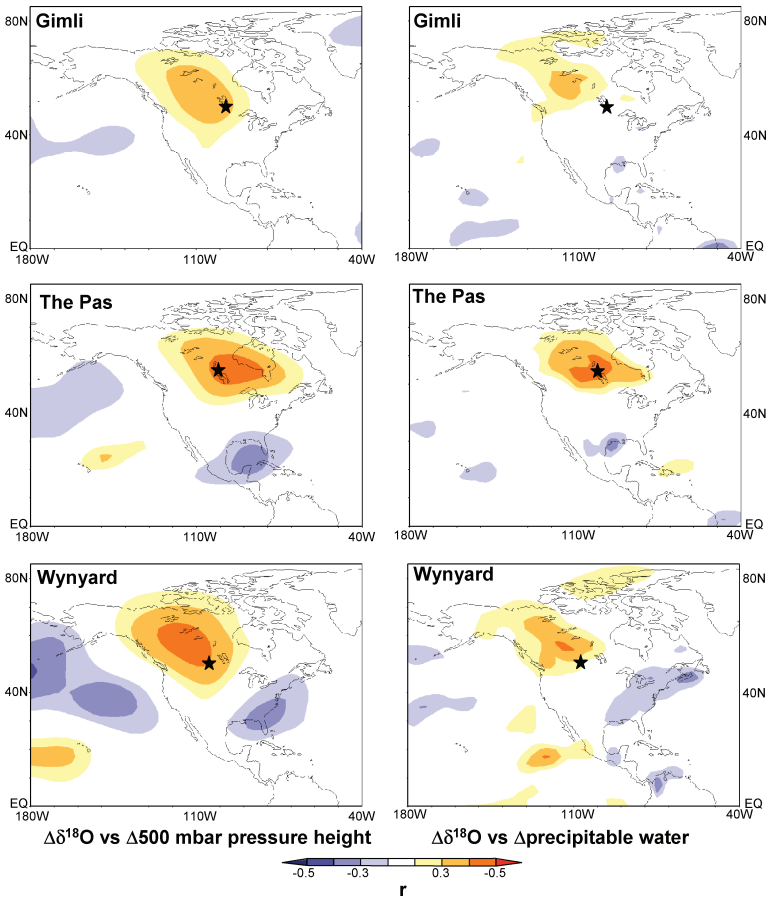

Fig. 6. Correlation between isotope anomalies at each station and 500 mbar pressure height (Δ500 mbh) and precipitable water (ΔPWAT) anomaly fields.

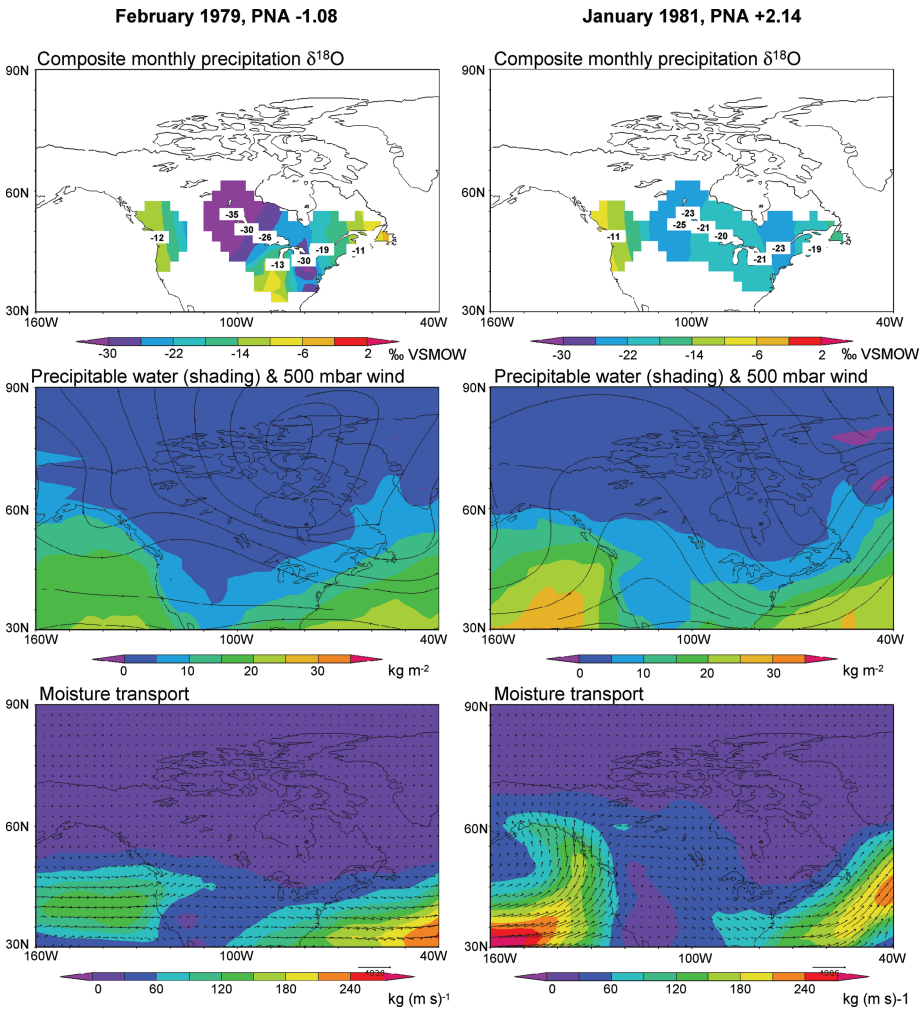

Fig. 7. Comparison of precipitation δ^{18}O fields with climate parameters for two winter months having strongly contrasting mid-tropospheric flow patterns. The contoured δ^{18}O data in the top panels are from the IAEA/WMO GNIP data base (IAEA/WMO, 2006).

evidence for the association of positive isotope anomalies when the ridge over western Canada is more pronounced, independent of the PNA index, was found in the positive correlations between individual monthly isotope anomalies at the three stations and positive pressure anomalies located over the Cordillera (Fig. 6). The correlations between isotope anomalies and temperature anomalies measured at each of the stations are not as strong as the same correlations with the PNA index, however, possibly because the PNA index integrates temperature anomalies not only at the station but also upstream along the air-mass trajectory.

Synoptic examples depicting isotope fields with the associated upper atmospheric parameters give a better indication of how changes in circulation alter rainout history than descriptive indices of circulation like the PNA. In the examples presented here, more depleted precipitation δ^{18}O values at our stations occurred when there was less precipitable water reaching the interior, indicating that a greater degree of rainout coincided with periods of more zonal flow across the continent. Intensified zonal flow, thus, deepens both the precipitation and isotope shadows in the lee of the Canadian Cordillera.

Fluctuations in the δ^{18}O–T relation are also linked to the PNA index, with higher slopes, lower intercepts and stronger correlations characterizing the relation during periods of sustained zonal flow, especially in winter. This suggests that a common moisture source and distillation history tend to dominate at such times. When flow is less zonal, atmospheric moisture delivered to western Canada has a more variable distillation history and, on average, a higher δ^{18}O for a given temperature.

5.2. *Past isotope climatology*

The latter observation has important implications for the calibration and application of precipitation δ^{18}O as a palaeothermometer since circulation-dependent effects may add additional signals that are not directly related to changes in temperature.

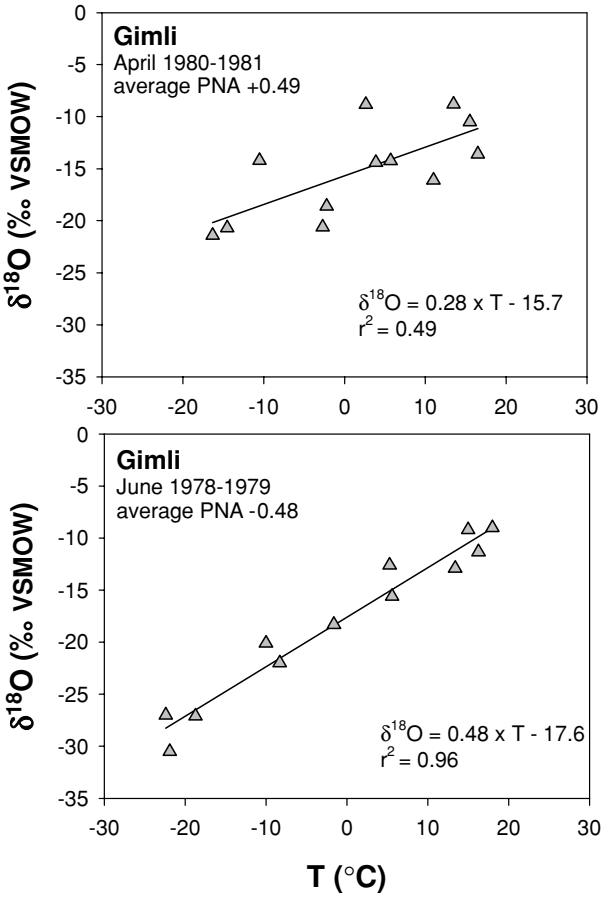

Fig. 8. Comparison of two 12-month time periods at Gimli having contrasting atmospheric circulation.

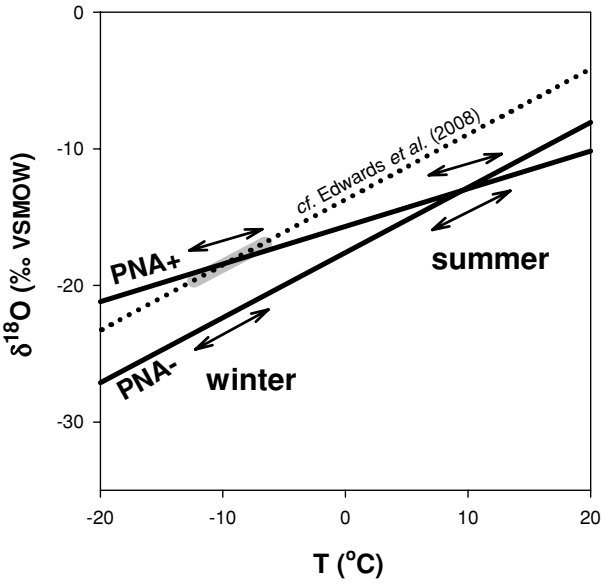

Fig. 9. Schematic δ^{18}O–*T* diagram based on the observed relations shown in Fig. 8 for Gimli in 1978–79 (PNA–) and 1980–81 (PNA+). The grey shaded zone on the dotted line indicates the nature of the approximation employed by Edwards et al. (2008) to account for apparent suppression of temperature-dependent effects on winter precipitation δ^{18}O during the Little Ice Age in western Canada, which was marked by persistence of meridional circulation (PNA+).

Indeed, these results are in harmony with mounting evidence that analogous circulation-dependent variability is a key feature of the isotopic labelling of palaeoprecipitation in western Canada over varying timescales. This includes δ^{18}O palaeorecords from lake sediments in north-central Canada (Edwards et al., 1996) and southern Yukon Territory (Anderson et al., 2005) spanning many millennia, as well as δ^{18}O palaeorecords from glacial ice in southern Yukon (Fisher et al., 2004) and tree-ring cellulose in southwestern Alberta (Edwards et al., 2008) spanning multiple centuries. Edwards et al. (2008), for example, suggested that spruce and pine near alpine treeline in the eastern Rocky Mountains inherited signals from winter snowmelt during the Little Ice Age (∼AD 1530s–1890s), which was relatively rich in ^{18}O, in spite of cooler average temperatures, because of intensified meridional circulation at this time. The proposed mechanism to explain this feature can be readily illustrated in the framework of the different temporal δ^{18}O–*T* relations observed at Gimli for PNA+ and PNA– circulation regimes, with the 'isotope thermometer' essentially offset during the Little Ice Age (Fig. 9), thereby suppressing the expected temperature-dependent depletion of ^{18}O in snowmelt. It is also evident from this model that the seasonality of precipitation captured in a palaeo-isotope archive influences sensitivity to circulation-dependent effects. As a result, potential may exist to couple palaeo-isotope data from archives that sample precipitation from different seasons to tease apart temperature- and circulation-dependent signals in the past.

6. Conclusions

Temperature clearly exerts primary control on the isotopic labelling of precipitation in western Canada, yet systematic variability in distillation history related to prevailing modes of large-scale atmospheric circulation also plays an important secondary role, especially for winter precipitation. Although our analysis is based on only 7 yr of monitoring from the late–20th-century, the sense and magnitude of the circulation-dependent effects are comparable to those inferred from various palaeorecords in the region, and hence may have broad applicability. The recent re-establishment of ongoing precipitation monitoring at a new network of sites (Birks et al., 2004) also affords the opportunity to undertake further analysis and testing under the slightly differing climatic conditions of the early–21st-century.

7. Acknowledgment

This research has been supported by Postdoctoral Fellowship (SJB) and Discovery Grant (TWDE) funding from the Natural Sciences and Engineering Research Council of Canada.

References

Amundson, R. G., Chadwick, O. A., Kendall, C., Wang, Y. and DeNiro, M. J. 1996. Isotopic evidence for shifts in atmospheric circulation patterns during the late Quaternary in mid-North America. *Geology* **24**, 23–26.

Anderson, L., Abbott, M. B., Finney, B. P. and Burns, S. J. 2005. Regional atmospheric circulation change in the North Pacific during the Holocene inferred from lacustrine carbonate oxygen isotopes, Yukon Territory, Canada. *Quat. Res.* **64**, 21–35.

Barnston, A. G. and Livezey, R. E. 1987. Classification, seasonality, and persistence of low-frequency atmospheric circulation patterns. *Mon. Wea. Rev.* **115**, 1083–1126.

Birks, S. J., Edwards, T. W. D., Gibson, J. J., Drimmie, R. J. and Michel, F. A. 2004. Canadian Network for Isotopes in Precipitation. Available at: http://www.science.uwaterloo.ca/twdedwar/cnip/cniphome.html

Cole, J. E., Rind, D. and Fairbanks, R. G. 1993. Isotopic responses to interannual climate variability simulated by an atmospheric general circulation model. In: *Decadal to Millennial-scale Variability in the Climate System* (eds. D. Murray and J. Overpeck). Pergamon, Oxford, 387–406.

Dansgaard, W. 1964. Stable isotopes in precipitation. *Tellus* **16**, 436–468.

Davis, R. E. and Benkovic, S. R. 1994. Spatial and temporal variations of the January circumpolar vortex over the Northern Hemisphere. *Int. J. Climatol.* **14**, 415–428.

Ecoregions Working Group. 1989. *Ecoclimatic Regions of Canada, First Approximation* (plus map at 1 : 750,000). Environment Canada, Ottawa, Canada, 119 pp.

Edwards, T. W. D., Wolfe, B. B. and MacDonald, G. M. 1996. Influence of changing atmospheric circulation on precipitation δ^{18}O-temperature relations in Canada during the Holocene. *Quat. Res.* **46**, 211–218.

Edwards, T. W. D., Birks, S. J., Luckman, B. H. and MacDonald, G. M. 2008. Climatic and hydrologic variability during the past millennium in the eastern Rocky Mountains and northern Great Plains of western Canada. *Quat. Res.* **70**, 188–197.

Fisher, D. A., Wake, C., Kreutz, K., Yalcin, K., Steig, E. and co-authors. 2004. Stable isotope records from Mount Logan, Eclipse ice cores and nearby Jellybean Lake. Water cycle of the North Pacific over 2000 years and over five vertical kilometres: sudden shifts and tropical connections. *Géographie physique et Quaternaire* **58**, 337–352.

Fricke, H. and O'Neil, J. 1999. The correlation between ^{18}O/^{16}O ratios of meteoric water and surface temperature: its use in investigating terrestrial climate change over geologic time. *Earth Planet. Sci. Lett.* **170**, 181–196.

Fritz, P., Drimmie, R. J., Frape, S. K. and O'Shea, K. J. 1987. The isotopic composition of precipitation and groundwater in Canada. In: *Isotope Techniques in Water Resources Development*. International Atomic Energy Agency, Vienna, 539–550.

Hammarlund, D. and Edwards, T. W. D. 2008. Stable isotope variations in stalagmites from northwestern Sweden document changes in temperature and vegetation during the early Holocene: a comment on Sundqvist *et al. 2007*. *Holocene* **18**, 1007–1008.

Hammarlund, D., Barnekow, L., Birks, H. J. B., Buchardt, B. and Edwards, T. W. D. 2002. Holocene changes in atmospheric circulation recorded in the oxygen-isotope stratigraphy of lacustrine carbonates from northern Sweden. *Holocene* **12**, 339–351.

Hoffmann, G., Jouzel, J. and Johnsen, S. 2001. Deuterium excess record from central Greenland over the last millennium: hints of a North Atlantic signal during the Little Ice Age. *J. Geophys. Res.—Atmospheres* **106**, 14265–14274.

Holdsworth, G. 2008a. A composite isotopic thermometer for snow. *J. Geophys. Res.* **113**, D08102, doi:10.1029/2007JD008634.

Holdsworth, G. 2008b. Interpreting H_2O isotope variations in high-altitude ice cores using a cyclone model. *J. Geophys. Res.* **113**, D08103, doi:10.1029/2007JD008639.

IAEA/WMO 2006. *Global Network of Isotopes in Precipitation*. The GNIP Database. Available at: http://isohis.iaea.org.

Jouzel, J. 1999. Calibrating the isotopic paleothermometer. *Science* **286**, 910–911.

Kalnay, E., Kanamitsu, M., Kistler, R., Collins, W., Deaven, D. and co-authors. 1996. The NCEP/NCAR 40-year reanalysis project. *Bull. Am. Meteorol. Soc.* **77**, 437–471.

Kohn, M. J. and Welker, J. M. 2005. On the temperature correlation of δ^{18}O in modern precipitation. *Earth Planet. Sci. Lett.* **231**, 87–96.

Lawrence, J. R. and White, J. W. C. 1991. The elusive climate signal in the isotopic composition of precipitation. In: *Stable Isotope Geochemistry: A Tribute to Samuel Epstein* Volume 3 (eds. H. P. Taylor, J. R. O'Neil and I. R. Kaplan). . The Geochemical Society Special Publication, 169–185.

Lee, J.-E., Fung, I., DePaolo, D. J. and Henning, C. C. 2007. Analysis of the global distribution of water isotopes using the NCAR atmospheric general circulation model. *J. Geophys. Res.* **112**, D16306, doi:10.1029/2006JD007657.

Lipp, J., Trimborn, P., Edwards, T. W. D., Waisel, Y. and Yakir, D. 1996. Climatic effects on the δ^{18}O and δ^{13}C of cellulose in the desert tree *Tamarix jordanis*. *Geochimica et Cosmochimica Acta* **60**, 3305–3309.

Moran, T. A., Marshall, S. J., Evans, E. C. and Sinclair, K. E. 2007. Altitudinal gradients of stable isotopes in lee-slope precipitation in the Canadian Rocky Mountains. *Arctic Antarctic Alpine Res.* **39**, 455–467.

Noone, D. and Simmonds, I. 1998. Implications for interpretations of ice-core isotope data from analysis of modelled Antarctic precipitation. *Ann. Glaciol.* **27**, 398–402.

Noone, D. and Simmonds, I. 2002. Associations between δ^{18}O of water and climate parameters in a simulation of atmospheric circulation for 1979–1995. *J. Clim.* **15**, 3150–3169.

Peng, H., Mayer, B., Harris, S. and Krouse, H. R. 2004. A 10-year record of stable isotope ratios of hydrogen and oxygen in precipitation at Calgary, Alberta, Canada. *Tellus* **56B**, 147–159.

Plummer, L. N. 1993. Stable isotope enrichment in paleowaters of the southeast Atlantic coastal plain, United States. *Science* **262**, 2016–2020.

Rozanski, K., Araguás-Araguás, L. and Gonfiantini, R. 1993. Isotopic patterns in modern global precipitation. In: *Climate Change in Continental Isotopic Records, Geophysical Monograph* Volume 78 (eds. P. K. Swart, K. C. Lohmann, J. McKenzie and S. Savin). American Geophysical Union, Washington, 1–36.

Salamatin, A. N., Lipenkov, V. Y., Barkov, N. I., Jouzel, J., Petit, J. R. and co-authors. 1998. Ice core age dating and paleothermometer calibration based on isotope and temperature profiles from deep boreholes at Vostok Station (East Antarctica). *J. Geophys. Res.—Atmospheres* **103**, 8963–8977.

Simpkins, W. W. 1995. Isotopic composition of precipitation in central Iowa. *J. Hydrol.* **172**, 185–207.

Smith, M. A. and Hollander, D. J. 1999. Historical linkage between atmospheric circulation patterns and the oxygen isotopic record of sedimentary carbonates from Lake Mendota, Wisconsin, USA. *Geology* **27**, 589–592.

Sturm, K., Hoffmann, G., Langmann, B. and Stichler, W. 2005. Simulation of δ^{18}O in precipitation by the regional circulation model REMOiso. *Hydrol. Process.* **19**, 3425–3444.

Sturm, C., Vimeux, F. and Krinner, G. 2007. Intraseasonal variability in South America recorded in stable water isotopes. *J. Geophys. Res.* **112**, D20118, doi:10.1029/2006JD008298.

Teranes, J. L. and McKenzie, J. A. 2001. Lacustrine oxygen isotope record of 20th-century climate change in central Europe: evaluation of climatic controls on oxygen isotopes in precipitation. *J. Paleolimnol.* **26**, 131–146.

Wallace, J. M. and Gutzler, D. S. 1981. Teleconnections in the geopotential height field during the Northern Hemisphere winter. *Mon. Wea. Rev.* **109**, 784–812.

Werner, M. and Heimann, M. 2002. Modeling interannual variability of water isotopes in Greenland and Antarctica. *J. Geophys. Res.—Atmospheres* **107**, doi:10.1029/2001JD900253.

Werner, M., Mikolajewicz, U., Heimann, M. and Hoffmann, G. 2000. Borehole versus isotope temperatures on Greenland; seasonality does matter. *Geophys. Res. Lett.* **27**, 723–726.